RSC Advances

PAPER

View Article Online
View Journal | View Issue

Open Access Article. Published on 14 October 2020. Downloaded on 1/21/2026 2:04:22 AM.
This article is licensed under a Creative Commons Attribution-NonCommercial 3.0 Unported Licence.

Check for updates

Cite this: *RSC Adv.*, 2020, **10**, 38038

Novel rhodamine dye with large Stokes shifts by fusing the 1,4-diethylpiperazine moiety and its applications in fast detection of Cu^{2+}†

Jin Gong,[ab] Chang Liu,[a] Xiaojie Jiao,[a] Song He,[a] Liancheng Zhao[ab] and Xianshun Zeng *[ab]

Received 4th July 2020
Accepted 6th October 2020

DOI: 10.1039/d0ra05835a

rsc.li/rsc-advances

Rhodamine dyes were widely developed for designing probes due to their excellent photophysical properties and biocompatibility. However, traditional rhodamine dyes still bear major drawbacks of short emission wavelengths (<600 nm) and narrow Stokes shifts (<30 nm), which limit their biological imaging applications. Herein, we reported a novel mitochondria-targeted fluorescent dye **JRQ** with near-infrared (NIR) emission wavelength and improved Stokes shift (63 nm) by tuning the donor–acceptor–donor (D–A–D) character of the rhodamine skeleton. As expected, **JRQ** exhibited multiple excellent properties and could accumulate in mitochondria, and can therefore be used as a signal reporter for the design of fluorescent probes by taking advantage of the fluorescence controlled mechanism of the ring opening and closing chemical processes of the spirolactone platform. By using **JRQ** as a precursor, a highly sensitive fluorescent probe **JRQN** for the fast detection of mitochondrial Cu^{2+} ions was synthesized based on the Cu^{2+}-triggered specific hydrolysis mechanism because mitochondria are an important reservoir of intracellular Cu^{2+}. We expect that the Stokes shift increase of rhodamine dyes *via* tuning the donor–acceptor–donor (D–A–D) character of the rhodamine skeleton will provide a novel synthetic approach for the development of rhodamine dyes and expansion of their applications.

Introduction

Rhodamine derivatives were widely developed for designing probes due to their excellent photophysical properties and biocompatibility, such as tolerance to photobleaching, high quantum yields, and distinct photophysical advantages of ring-opening process.[1] However, traditional rhodamine-based probes still bear some major drawbacks, such as short emission wavelengths (<600 nm) and narrow Stokes shifts (<30 nm), which are the main reasons for self-quenching, excitation wavelength interference and photodamage in living cells.[2] Next generation applications, *e.g.* single-molecule analysis, demand fluorescent probes with NIR emission wavelength and large Stokes shifts to achieve precise imaging and accurate sensing.[3] To data, several strategies have been introduced to increase the emission wavelength, for example, extending the π-conjugated system of rhodamine scaffolds and replacing the bridging oxygen atom with other atoms.[4] However, these strategies cannot effectively improve the Stokes shifts. Therefore, it is of great significance to design and synthesize new rhodamine dyes with near-infrared (NIR) emission wavelengths and large Stokes shifts.

Recently, it has been reported that altering the intramolecular charge transfer (ICT) properties of chromophoric skeleton by tuning electron-donating character of the chromophore is an efficient strategy to increase the absorption and emission wavelengths of rhodamine dyes.[5] In pioneering works, the emission wavelengths of dyes were prominently red-shifted by fusing a piperazine in the xanthene skeleton as strong electron-donating group, increased with the Stokes shifts.[6] For example, Zhang and coworkers demonstrated that the emission wavelengths of rhodamine dyes are prominently red-shifted by using the 1,4-diethyl-1,2,3,4-tetrahydroquinoxaline unit as a strong electron-donating group to modify the xanthene moiety, increased with the Stokes shifts.[6a] In 2018, Luck and Liu *et al.* reported the incorporation of a piperazine fused ring on the rhodamine scaffold, which also both increased the emission wavelengths and the Stokes shifts.[6b] These results have inspired our synthetic efforts aimed at the development of new rhodamine dyes with NIR emission wavelengths and improved Stokes shifts.

In this paper, we design of a new rhodamine dye with NIR emission wavelengths and larger Stokes shifts by introducing the electron-donating 1,4-diethylpiperazine moiety in

[a]*Tianjin Key Laboratory for Photoelectric Materials and Devices, School of Materials Science & Engineering, Tianjin University of Technology, Tianjin, 300384, China. E-mail: xshzeng@tjut.edu.cn*

[b]*School of Materials Science and Engineering, Harbin Institute of Technology, Harbin, 150001, China*

† Electronic supplementary information (ESI) available. See DOI: 10.1039/d0ra05835a

This journal is © The Royal Society of Chemistry 2020

Open Access Article. Published on 14 October 2020. Downloaded on 1/21/2026 2:04:22 AM.
This article is licensed under a Creative Commons Attribution-NonCommercial 3.0 Unported Licence.

rhodamine scaffold for tuning the D–A–D character of rhodamine dyes. In addition, the cationic xanthene moiety normally works as a functional group for targeting mitochondria,[7] and increase the water solubility of the dye. As expected, **JRQ** exhibited multiple excellent properties and was capable of specifically distributing in mitochondria, which can be used as signal reporter for the design of fluorescence probes by taking advantage of the fluorescence controlled mechanism of the ring opening and closing chemical processes of the spirolactone platform. Furthermore, to demonstrate the utility of this dye for probe design, a highly sensitive and selective fluorescent probe **JRQN** for the specific detection of mitochondrial Cu^{2+} ions was synthesized based on the Cu^{2+}-triggered specific hydrolysis mechanism because mitochondria are important reservoir of intracellular Cu^{2+}.

Results and discussion

Molecular synthesis

The dye **JRQ** and probe **JRQN** were synthesized according to the procedures in Scheme 1. The intermediate compounds 4-methoxy-1,2-phenylenediamine (**A**), 1,4-diethyl-6-methoxy-1,2,3,4-tetrahydroquinoxaline (**B**) and 2-(2-hydroxyjulolidine) benzoic acid (**C**) were synthesized according to the literature,[6a,8] and the detailed reaction reagents and conditions were depicted in Scheme 1. By the reaction of 2-(4-diethylamino-2-hydroxybenzoyl)benzoic acid with **B**, the dye **JRQ** was obtained in 76% yield. Followed by the reaction of the dye **JRQ** with hydrazine hydrate in methanol, the probe **JRQN** was obtained in 53% yield. The structures of the new compounds **JRQ** and **JRQN** were characterized by spectroscopic techniques, for example, ^{1}H NMR, ^{13}C NMR and HRMS, and the spectra were presented in the ESI† in detail.

Characterization of JRQ

In order to verify whether **JRQ** meets our original design intentions, a detailed evaluation of the photophysical properties of the dye **JRQ** in distinct solvents (CH_3CN, DMSO, DCM, EtOH, and H_2O) was conducted. Surprisingly, **JRQ** showed the maxima absorption bands between 583 nm and 590 nm ($\varepsilon \geq$ 14 200 M^{-1} cm^{-1}), and the maxima emission peaks of **JRQ** range from 654 nm to 668 nm in all test solvents (Table S1 and Fig. S1†). Comparatively, **JRQ** showed longer emission and larger Stokes shift than traditional rhodamine dyes in ethanol (Table 1). The maximum fluorescence emission of the dye was remarkably red-shifted *ca.* 61 nm (rhodamine 101), 86 nm (rhodamine B), and 100 nm (rhodamine 6G), respectively, which may be attributed to the excited intramolecular charge transfer (ICT). Meanwhile, the Stokes shift of **JRQ** was calculated to be 63 nm in ethanol, which was significantly larger than rhodamine 101 (30 nm), rhodamine B (26 nm), and rhodamine 6G (28 nm), respectively. It can be rationalized that the change of the electron-donating 1,4-diethylpiperazine group in the asymmetric xanthene fluorophore can regulate the donor–acceptor–donor (D–A–D) character of the chromophore. The donor–acceptor system in plane from the electron-donating 1,4-diethylpiperazine group to the electron-withdrawing group in **JRQ** can lead to large changes in the energy difference between the ground and the excited state, thereby producing an obviously increased Stokes shifts.[9] Furthermore, the quantum yields of **JRQ** range from 5% to 54% in these solvents (Table S1†). Collectively, it proved that **JRQ** was a novel NIR fluorescence reagent with large Stokes shift, achieving original design intentions.

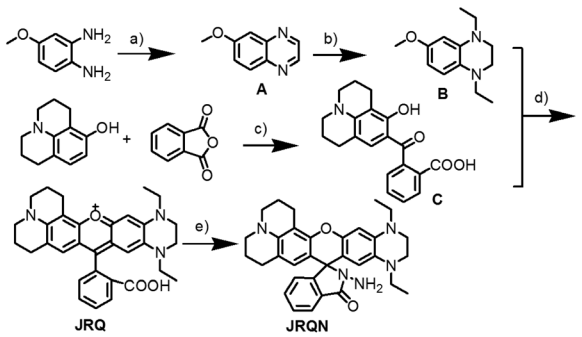

Scheme 1 Synthesis of dye **JRQ** and probe **JRQN**. Reagents and conditions: (a) succinaldehyde, CH_3CN, 60 °C, overnight; (b) $NaBH_4$, toluene, AcOH, 5 °C to reflux, 5 h; (c) toluene, reflux, overnight; (d) CH_3SO_3H, 80 °C, 8 h; (e) NH_2NH_2, MeOH, 50 °C, 6 h.

Fluorescent imaging of JRQ

The excellent photophysical properties, for example, NIR emission wavelengths and improved Stokes shifts, encouraged us to examine the potential applications of **JRQ** in living cells. Before the imaging experiments in living cells, the well-established MTT assay was adopted to study cytotoxicity of the aforementioned dye at varying concentrations (0, 1, 3, 5, 10, and 20 μM). As shown in Fig. S2,† more than 85% of cells survived after treatment with various concentrations of **JRQ** (0, 1, 3, 5, 10, and 20 μM) for 24 h, indicated that the dye has fairly low toxicity to living cells. Then imaging experiments of **JRQ** in living cells were carried out. HeLa cells were incubated with **JRQ** for 30 min, and then washed three times with PBS for removing excess reagents in the growth medium. As shown in Fig. S3,† strong red fluorescence signals were observed after treatment with **JRQ** (1 μm) for 30 min, indicating that the dye was membrane permeability and could be used for imaging in living cells.

By carefully observing the overlap images, we found that the distribution of the red signal in the cells unevenly fill the entire cytoplasm, but concentrated in some regions, indicating that **JRQ** likely possessed organelles localization properties.

Table 1 λ_{ex} and λ_{em} values of **JRQ**, rhodamine 101, rhodamine B and rhodamine 6G in EtOH

Dyes	λ_{ex} (nm)	λ_{em} (nm)	$\Delta\lambda$ (nm)
Rhodamine 101	564	594	30
Rhodamine B	543	569	26
Rhodamine 6G	527	555	28
JRQ	592	655	63

Open Access Article. Published on 14 October 2020. Downloaded on 1/21/2026 2:04:22 AM.
This article is licensed under a Creative Commons Attribution-NonCommercial 3.0 Unported Licence.

According to the literature, the xanthene dyes leads to the proactive accumulation in mitochondria,[7] therefore, **JRQ** was likely to accumulate in mitochondria. To verify the speculated organelles localization properties, the co-localization experiments through co-incubating the HeLa cells with commercial targeting reagents Mito-Tracker Green (Mito), Golgi-Tracker Green (Golgi), ER-Tracker Green (ER), and Lyso-Tracker Green (Lyso), respectively, were conducted. As expected, highlight yellow pixels on overlapping images were observed in Fig. 1a, and a high overlap coefficient (0.92) and Pearson's coefficient (0.91) could be calculated from the intensity correlation plot, suggesting that **JRQ** was mainly distributed in mitochondria. In contrast, red fluorescence signals of **JRQ** and green fluorescence signals of other trackers (Lyso, ER, or Golgi) were distinctly distributed in different regions, and low overlap coefficients and Pearson's coefficients were observed (Table S2†), indicating that **JRQ** does not accumulate in these organelles. Co-localization experiments confirmed that **JRQ** can be used as an effective mitochondrial targeting reagent.

Recognition properties of JRQN

Copper is a redox-active metal that has a wide range of applications in the chemical and electronics industries, and plays an indispensable role in various physiological processes as enzyme cofactors and signal messengers, including cellular respiration, neurotransmitter synthesis and metabolism, maintenance of the immune system, redox process, bone health, *etc.*[10] As a cofactor for the respiratory enzyme cytochrome c oxidase, mitochondria are important reservoir of intracellular copper.[11] Therefore, humans must supplement their normal intake by means of food, and the average daily copper intake of adults should not exceed 10–12 mg.[12] It has been proved that abnormal levels of copper (Cu^{2+}) in the body can cause diseases, for example, Alzheimer's disease, coronary heart disease, Wilson's disease, arthritis, brain dysfunction, anemia, Menkes disease and vitiligo.[13] Consequently, real-time sensing Cu^{2+} levels in mitochondria is important for early detection and prevention of diseases. However, up to now, mitochondria-targeted NIR fluorescent probes of rhodamine derivatives with large Stokes shifts for detection of Cu^{2+} were rarely described.[14] Therefore, it is of great significance to design and synthesize new NIR fluorescent probes with large Stokes shifts, for sensing Cu^{2+} in mitochondria.

To demonstrate the utility of this dye for probe design, a highly sensitive fluorescent probe **JRQN** for the fast detection of mitochondrial Cu^{2+} ions was synthesized based on the Cu^{2+}-triggered specific hydrolysis mechanism because mitochondria are important reservoir of intracellular Cu^{2+}.[15] With **JRQN** in hand, the different metalated analogues were evaluated, in order to study the influence of the metals on the absorption and emission spectrum of the probe. As shown in the Fig. 2a, upon addition of 10 equiv. of Cu^{2+}, the intensity of the fluorescence emission spectrum at 678 nm was significantly enhanced, which could be attributed to the formation of large π–π conjugated system through Cu^{2+}-triggered ring-opening and hydrolysis cascade reaction.[15] In contrast, no significant change in the fluorescence emission spectrum was observed after addition of 10 equiv. other metal cations (Ag^{+}, Al^{3+}, Ca^{2+}, Fe^{2+}, Cd^{2+}, Co^{2+}, Cr^{3+}, Fe^{3+}, Mg^{2+}, K^{+}, Li^{+}, Mn^{2+}, Pd^{2+}, Na^{+}, Ni^{2+}, and Zn^{2+}). Meanwhile, the same trend was also exhibited in the absorption spectrum (Fig. S4†). Upon addition of 10 equiv. of Cu^{2+}, the absorption intensity of **JRQN** at 594 nm was significantly enhanced. In contrast, no obvious responses of absorption spectrum were observed after addition of various other metal cations under the same conditions. In addition, the probe can also respond to high concentration of Hg^{2+} (Fig. S5†). Considering that the cells do not contain Hg^{2+}, the recognition of Cu^{2+} in the living cells will not be affected. Accordingly, intense absorption (λ_{abs} = 594 nm) and fluorescence emission (λ_{em} = 678 nm) appear, indicating the formation of highly

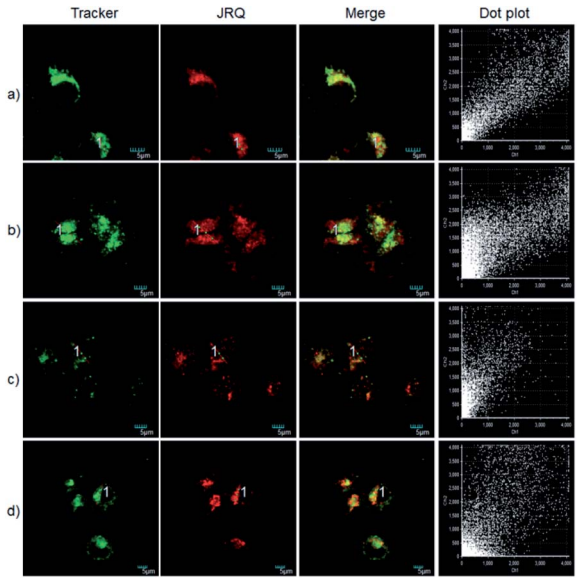

Fig. 1 Co-localization experiments with HeLa cells stained with **JRQ** (1 μM) and other organelle-targeting Trackers (200 nM). (a) Costained with Mito-Tracker Green; (b) costained with Lyso-Tracker Green, (c) costained with ER-Tracker Green; (d) costained with Golgi-Tracker Green. Red channel: λ_{ex} = 559 nm, λ_{em} = 618–718 nm; green channel: λ_{ex} = 488 nm, λ_{em} = 520–541 nm.

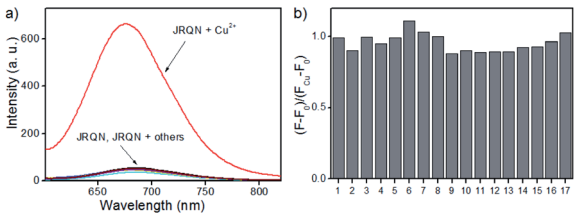

Fig. 2 (a) Fluorescence emission responses of **JRQN** (10 μM) upon addition of different species; (b) fluorescence ratio ($(F - F_0)/(F_{Cu} - F_0)$) changes of **JRQN** in the presence of 100 μM Cu^{2+} and different species. Metal cations (100 μM): (1) Ag^{+}; (2) Al^{3+}; (3) Ca^{2+} (10 mM); (4) Cd^{2+}; (5) Co^{2+}; (6) Cr^{3+}; (7) Cu^{2+}; (8) Fe^{2+}; (9) Fe^{3+}; (10) Pd^{2+}; (11) K^{+} (10 mM); (12) Li^{+} (10 mM); (13) Mg^{2+} (10 mM); (14) Mn^{2+}; (15) Na^{+}; (16) Ni^{2+}; (17) Zn^{2+}. The conditions: HEPES buffer (10 mM, pH = 7.4, containing 20% CH_3CN), λ_{ex} = 580 nm, slit = 5/5 nm.

Open Access Article. Published on 14 October 2020. Downloaded on 1/21/2026 2:04:22 AM.
This article is licensed under a Creative Commons Attribution-NonCommercial 3.0 Unported Licence.

fluorescent ring-opening form after the reaction of **JRQN** and Cu^{2+}. The Stokes shift of **JRQN** was found to be 84 nm, which was obviously larger than those of conventional rhodamine dyes (<30 nm).[16] The results revealed that **JRQN** can function as a highly selective fluorescence probe for Cu^{2+}. To verify the speculated mechanism, HRMS was conducted to analyze the change of molecular weight of **JRQN** after the reaction with Cu^{2+}. As shown in Fig. S6,† an intense peak at *m*/*z* 508.2600 corresponding to **JRQ** was distinct after the reaction of **JRQN** with Cu^{2+}, revealing that the open-ring and hydrolysis cascade reaction process was triggered and the carboxylic acid compound **JRQ** was constructed.

Subsequently, competitive experiments were conducted to assess whether the interfering metal ions showed interference with the detection of Cu^{2+}. It was investigated that the response signal of **JRQN** towards Cu^{2+} in the presence of 10 equiv. coexistent potentially interfering metal ions (Ag^+, Al^{3+}, Ca^{2+}, Fe^{2+}, Cd^{2+}, Co^{2+}, Cr^{3+}, Fe^{3+}, Mg^{2+}, K^+, Li^+, Mn^{2+}, Pd^{2+}, Na^+, Ni^{2+}, and Zn^{2+}). As shown in Fig. 2b, all of the tested foreign metal ions had minor or no interference with signal response to Cu^{2+} and **JRQN** exhibited obvious response even in the presence of interfering metal species, revealing that interfering metal species had minor or no interference to the selective recognition properties of **JRQN**. Therefore, results of competition experiments further confirming the specificity of **JRQN** toward Cu^{2+}.

In order to assess the sensitivity of **JRQN** towards Cu^{2+}, continuous titration experiments were conducted by using fluorescence and UV/Vis spectroscopy. As shown in Fig. 3a, after the addition of increasing concentration of Cu^{2+} (0–105 μM), the fluorescent maximum at 678 nm remarkably increased, and eventually reached constant when the amount of Cu^{2+} reached 10 equiv. Subsequently, the linear fitting could be obtained between Cu^{2+} concentrations ranging from 0 to 30 μM and the fluorescence emission intensity at 678 nm with an excellent linear relationship (R = 0.9977) (Fig. 3b). Then, the detection limit of **JRQN** towards Cu^{2+} was obtained to be 29 nM based on the equation of $3\sigma/k$, where k is the slope plotted from the fitting equation mentioned above and σ is the relative standard deviation of 10 times fluorescence measurements of the blank solution in parallel without Cu^{2+}. The detection limit was far lower than the maximum allowable level of the World Health Organization (WHO) limit (30 μM)[17] and the U.S. Environmental Protection Agency's (EPA) limit for drinking water (20 μM).[18] At the same time, after the addition of increasing concentration of Cu^{2+} (0–10.5 equiv.), the absorption intensity of **JRQN** at 594 nm remarkably increased and reached the plateau when the amount of Cu^{2+} reached 5 equiv. (Fig. S7†). These results suggested that **JRQN** could be used as a practical probe for quantitative detection of Cu^{2+} in drinking water.

In order to evaluate whether **JRQN** was suitable for detecting Cu^{2+} in real time, time-dependent fluorescent responses of **JRQN** towards Cu^{2+} were evaluated by fluorescence spectroscopy at room temperature. The spectral data were recorded within 500 s in the absence and presence of Cu^{2+}. As shown in Fig. 4a, in the absence of Cu^{2+}, the fluorescence intensity of **JRQN** at 678 nm remained substantially constant, suggesting that the probe owned high photo-stability. In contrast, in the presence of Cu^{2+}, the fluorescence emission intensity of **JRQN** at 678 nm rapidly increased and reached a plateau within about 50 s, implying that **JRQN** could be used as an effective candidate for monitoring Cu^{2+} in real-time. In addition, in order to evaluate whether **JRQN** was suitable for detecting Cu^{2+} in physiological environment and find a suitable pH span in which **JRQN** could selectively detect Cu^{2+} efficiently, the emission spectra of **JRQN** in the absence and presence of Cu^{2+} at different pH values were measured. As illustrated in Fig. 4b, in the absence of Cu^{2+}, fluorescence intensity of **JRQN** at 678 nm remained substantially constant under a pH range of 6.0–10.0, while high fluorescence was observed under acidic conditions (4.0–5.0) for ring-opening induced by H^+. In contrast, in the presence of Cu^{2+}, the fluorescence intensity at 678 nm was obviously enhanced in the pH range of 5.0–10.0 for the ring-opening induced by Cu^{2+}, implying that **JRQN** could be used for detecting Cu^{2+} under physiological conditions. Collectively, above results suggested that **JRQN** was ability to detect trace amount of Cu^{2+} in real-time in physiological environments.

Fluorescent imaging of JRQN in HeLa cells

The spectral properties confirmed that **JRQN** had advantages of high selectivity, high sensitivity and fast response time for Cu^{2+} recognition, which encouraged us to examine the potential applications of **JRQN** for imaging Cu^{2+} in living cells. Before the imaging experiments in living cells, the well-established MTT assay was adopted to study cytotoxicity of the aforementioned

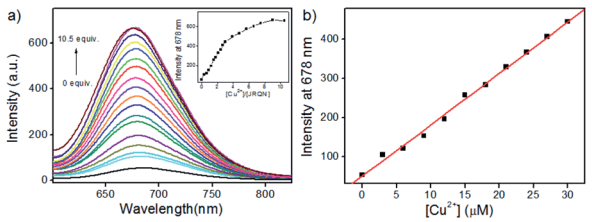

Fig. 3 (a) The fluorescence changes of **JRQN** (10 μM) treated with increasing concentrations of Cu^{2+} (0–105 μM). Inset: the plot of the fluorescence intensities at 678 nm *versus* the equivalents of Cu^{2+}; (b) the plot of the fluorescence intensities of **JRQN** at 678 nm *versus* the concentrations of Cu^{2+} (0–30 μM). The conditions: HEPES buffer (10 mM, pH = 7.4, containing 20% CH_3CN), λ_{ex} = 580 nm, slit = 5/5 nm.

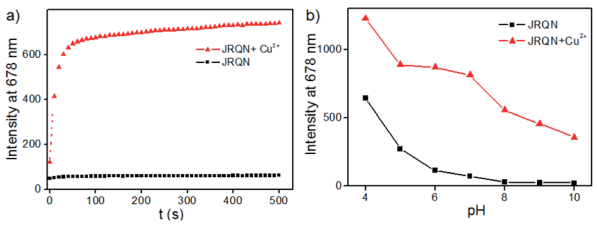

Fig. 4 (a) Time-dependence fluorescence intensity of **JRQN** (10 μM) upon addition of 100 μM Cu^{2+}; (b) fluorescence intensity of **JRQN** (10 μM) as a function of pH value in the absence/presence of Cu^{2+} (100 μM); the conditions: HEPES buffer (10 mM, pH = 7.4, containing 20% CH_3CN), λ_{ex} = 580 nm, slit = 5/5 nm.

Open Access Article. Published on 14 October 2020. Downloaded on 1/21/2026 2:04:22 AM.
This article is licensed under a Creative Commons Attribution-NonCommercial 3.0 Unported Licence.

probe at varying concentrations (0, 1, 3, 5, 10, and 20 μM). As shown in Fig. S8,† the viabilities of HeLa cells were not noticeably affected after incubation for 24 h, indicating low cytotoxicity of **JRQN**. Then, cell imaging of **JRQN** for monitoring of Cu^{2+} in living cells were carried out (Fig. 5). HeLa cells were incubated with **JRQN** for 30 min, and then washed three times with PBS for removing excess reagents in the growth medium. As shown in Fig. 5a, weak red fluorescence signals were observed in the red channel, implying the extremely low background of **JRQN**. In contrast, obvious enhancement fluorescence signals were observed in the red channel after treatment with Cu^{2+} (5 μm) for another 30 min under the same conditions (Fig. 5b). Compared with the controlled cells, the relative enhancement of fluorescence signals is about 5-fold (Fig. 5c). Results indicated that **JRQN** was membrane permeability and could be used for imaging Cu^{2+} in living cells.

By carefully observing the overlap images, we found that the distribution of the red signal in the cells unevenly fill the entire cytoplasm, but concentrated in some regions, indicating that **JRQN** likely possessed organelles localization properties. According to the literature, Cu^{2+} mainly accumulates in the mitochondria and lysosome of cells,[19] and the xanthene dyes leads to the proactive accumulation in mitochondria,[7] therefore, **JRQN** was likely to accumulate in one of the two organelles. To verify the speculated organelles localization properties, the co-localization experiments through co-incubating the HeLa cells with commercial targeting reagents Mito-Tracker Green (Mito), Golgi-Tracker Green (Golgi), ER-Tracker Green (ER), and Lyso-Tracker Green (Lyso), respectively, were conducted. As expected, highlight yellow pixels on overlapping images were observed in Fig. 6a, and a high overlap coefficient (0.93) and Pearson's coefficient (0.92) could be calculated from the intensity correlation plot, suggesting that **JRQN** was mainly distributed in mitochondria. In contrast, red fluorescence signals of **JRQN** and green fluorescence signals of other trackers (Lyso, ER, or Golgi) were distinctly distributed in different regions, and low overlap coefficients and Pearson's coefficients were obtained (Table S3†), indicating that **JRQN** does not accumulate in these organelles. Taken together, considering a series of excellent spectral properties and mitochondrial localization properties, the probe may be operated well in monitoring of Cu^{2+} concentration in the mitochondria for the relevant diseases.

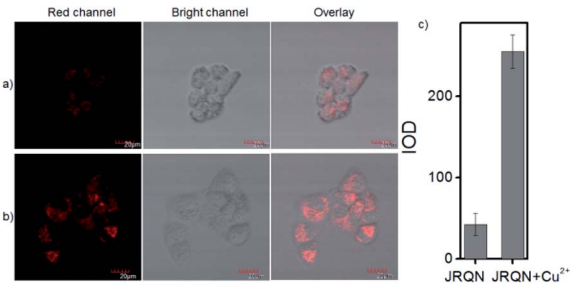

Fig. 5 (a) Fluorescent images of HeLa cells incubated with **RQS** (1 μM) for 30 min; (b) and then further incubated with Cu^{2+} (5 μM) for 30 min; (c) histogram of fluorescence enhancement. λ_{ex} = 559 nm, λ_{em} = 650–750 nm.

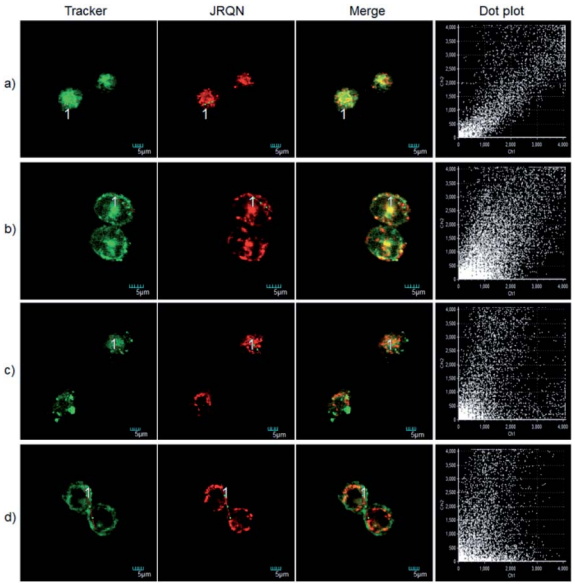

Fig. 6 Fluorescence imaging of the Cu^{2+}-pretreated HeLa cells being costained with **JRQN** (1 μM) and other organelle-targeting Trackers (200 nM). Cells were incubated with probes at 37 °C for 30 min, and then treated with Cu^{2+} (5 μM) for another 30 min. (a) Costained with Mito-Tracker Green; (b) costained with Lyso-Tracker Green, (c) costained with ER-Tracker Green; (d) costained with Golgi-Tracker Green. Red channel: λ_{ex} = 559 nm, λ_{em} = 650–750 nm; green channel: λ_{ex} = 488 nm, λ_{em} = 511–534 nm.

Conclusions

In summary, we reported a novel rhodamine dye (**JRQ**) with NIR emission wavelengths and larger Stokes shift by introducing the electron-donating 1,4-diethylpiperazine moiety in rhodamine scaffold for tuning the D–A–D character of rhodamine dyes. As expected, **JRQ** exhibited multiple excellent properties and was capable of specifically distributing in mitochondria, which can be used as signal reporter for the design of fluorescence probes by taking advantage of the fluorescence controlled mechanism of the ring opening and closing chemical processes of the spirolactone platform. Furthermore, to demonstrate the utility of this dye for probe design, a highly sensitive and selective fluorescent probe **JRQN** for the specific detection of mitochondrial Cu^{2+} ions was synthesized based on the Cu^{2+}-triggered specific hydrolysis mechanism because mitochondria are important reservoir of intracellular Cu^{2+}. **JRQN** was an outstanding "*turn-on*" fluorescence sensor with multiple excellent properties, and showed specifically distributing in mitochondrial regions, and thus detect Cu^{2+} in real-time there, which indicated that the probe can be used for monitoring intracellular mitochondria Cu^{2+} levels.

Experimental

Instruments and reagents

All reagents and organic solvents were commercially available in analytical grade, and were used directly without further purification. Compounds structures were characterized by

 This journal is © The Royal Society of Chemistry 2020

Open Access Article. Published on 14 October 2020. Downloaded on 1/21/2026 2:04:22 AM.
This article is licensed under a Creative Commons Attribution-NonCommercial 3.0 Unported Licence.

HRMS and NMR spectrometry. ^{1}H NMR (400 MHz) and ^{13}C NMR (100 MHz) spectra were measured by Bruker spectrometer using tetramethylsilane (TMS) as an internal standard. Agilent 6510 Q-TOF LC/MS instrument (Agilent Technologies, Palo Alto, CA) was used to measure molecular mass. UV-2550 UV/Vis spectrophotometer (Hitachi Japan) and F-4600 fluorescence spectrophotometer (Hitachi Japan) were used to collect spectroscopic properties. The pH was measured using a FE 20/EL 20 pH meter (Mettler-Toledo Instruments (Shanghai) Co., Ltd.). Fluorescent imaging was carried out by Olympus FV 1000-IX81 laser scanning confocal imaging.

Synthetic procedures

Synthesis A, B and C. 4-Methoxy-1,2-phenylenediamine (**A**), 1,4-diethyl-6-methoxy-1,2,3,4-tetrahydroquinoxaline (**B**) and 2-(2-hydroxyjulolidine) benzoic acid (**C**) were synthesized according to reported method.[6a,8]

Synthesis of JRQ. The compound **B** (2.2 g, 10 mmol) and **C** (3.7 g, 11 mmol) were dissolved in 5 mL methanesulfonic acid, and then the reaction system was heated to 80 °C and reacted under vigorous stirring for 8 hours. After cooling to room temperature, the mixture was extracted with DCM (50 mL × 3) and the collected organic layers were dried over anhydrous Na_2SO_4. The crude product was obtained by concentration under vacuum, and then purified by column chromatography to afford the compound **JRQ** as a blue solid (4.1 g) in 81% yield. ^{1}H NMR (400 MHz, $CDCl_3$) δ 8.35–8.25 (m, 1H), 7.54–7.47 (m, 2H), 7.07–7.01 (m, 1H), 6.67 (s, 1H), 6.59 (s, 1H), 5.96 (s, 1H), 3.61 (s, 2H), 3.55 (dd, J = 14.2, 7.1 Hz, 2H), 3.42–3.37 (m, 4H), 3.19 (s, 2H), 3.07–2.91 (m, 4H), 2.64–2.51 (m, 2H), 2.02 (d, J = 5.0 Hz, 2H), 1.87 (d, J = 5.7 Hz, 2H), 1.28 (t, J = 7.1 Hz, 3H), 0.87 (t, J = 7.2 Hz, 3H). ^{13}C NMR (100 MHz, $CDCl_3$) δ 166.59, 155.76, 153.64, 151.59, 149.71, 146.43, 134.50, 134.42, 133.19, 131.65, 131.24, 129.41, 129.38, 125.79, 123.50, 114.85, 113.87, 104.64, 104.05, 94.41, 50.72, 50.26, 48.02, 47.02, 45.43, 44.04, 27.72, 20.72, 20.05, 19.89, 10.99, 9.42. HRMS m/z = 508.2600 calcd for $C_{32}H_{34}N_3O_3$ $[M]^+$, found: 508.2609.

Synthesis of JRQN. Hydrazine hydrate (50 μL) was added to the methanol solution (10 mL) of **JRQ** (1.02 g, 2 mmol), and then the reaction system was heated to 50 °C and reacted under vigorous stirring for 6 hours. After cooling to room temperature, the mixture was extracted with DCM (50 mL × 3) and the collected organic layers were dried over anhydrous Na_2SO_4. The crude product was obtained by concentration under vacuum, and then purified by column chromatography to afford the compound **JRQN** as a pale yellow solid (0.55 g) in 53% yield. ^{1}H NMR (400 MHz, $CDCl_3$) δ 7.96–7.87 (m, 1H), 7.46–7.36 (m, 2H), 7.14–7.04 (m, 1H), 6.34 (s, 1H), 6.03 (s, 1H), 5.62 (s, 1H), 3.56 (d, J = 0.6 Hz, 2H), 3.40–3.29 (m, 4H), 3.13 (d, J = 7.6 Hz, 4H), 3.11–3.05 (m, 2H), 3.03–2.85 (m, 4H), 2.49 (qd, J = 15.9, 7.9 Hz, 2H), 2.08–1.98 (m, 2H), 1.86 (dt, J = 12.0, 6.2 Hz, 2H), 1.20 (t, J = 7.0 Hz, 3H), 0.83 (t, J = 7.0 Hz, 3H). ^{13}C NMR (100 MHz, $CDCl_3$) δ 166.25, 151.98, 149.03, 146.21, 143.53, 137.27, 132.32, 131.40, 129.79, 127.83, 123.94, 123.88, 122.87, 117.19, 107.70, 104.34, 104.24, 97.86, 66.90, 49.97, 49.51, 46.65, 45.74, 45.43, 45.35, 27.20, 22.02, 21.48, 21.28, 10.51, 9.61. HRMS m/z = 522.2895 calcd for $C_{32}H_{35}N_5O_2$ $[M + H]^+$, found: 522.2886.

Cell culture and fluorescence imaging

HeLa cells for imaging were cultured in DMEM medium supplemented with 10% (v/v) fetal bovine serum and penicillin/streptomycin (100 μg mL^{-1}) in an atmosphere of 5% CO_2 at 37 °C. HeLa cells were incubated with **JRQ** (1 μM) for 30 minutes. HeLa cells were incubated with **JRQN** (1 μM) for 30 minutes, and then Cu^{2+} (5 μM) was added and incubated for another 30 minutes. For co-localization experiments, **RQN** (1 μM) were incubated with 200 nM trackers (Mito-Tracker Green (Mito), Golgi-Tracker Green (Golgi), ER-Tracker Green (ER), and Lyso-Tracker Green (Lyso)) for 30 minutes, respectively; **JRQN** (1 μM) were incubated with 200 nM trackers (Mito-Tracker Green (Mito), Golgi-Tracker Green (Golgi), ER-Tracker Green (ER), and Lyso-Tracker Green (Lyso)) for 30 minutes, respectively, and then treated with Cu^{2+} (5 μM) for another 30 min. Fluorescence imaging was performed after washing the medium three times with PBS.

Conflicts of interest

There are no conflicts to declare.

Acknowledgements

This work was sponsored by the Natural Science Foundation of China (NNSFC 21907075; 21272172), and the Natural Science Foundation of Tianjin City (19JCZDJC32400; 18JCQNJC75900).

Notes and references

1 (*a*) M. Beija, C. A. M. Afonso and J. M. G. Martinho, *Chem. Soc. Rev.*, 2009, **38**, 2410; (*b*) D. T. Quang and J. S. Kim, *Chem. Rev.*, 2010, **110**, 6280; (*c*) X. Chen, T. Pradhan, F. Wang, J. S. Kim and J. Yoon, *Chem. Rev.*, 2012, **112**, 1910; (*d*) Y. Yang, Q. Zhao, W. Feng and F. Li, *Chem. Rev.*, 2012, **113**, 192; (*e*) K. P. Carter, A. M. Young and A. E. Palmer, *Chem. Rev.*, 2014, **114**, 4564; (*f*) S. Cai, Y. Lu, S. He, F. Wei, L. Zhao and X. Zeng, *Chem. Commun.*, 2013, **49**, 822.

2 (*a*) Z. Zhang and S. Achilefu, *Org. Lett.*, 2004, **6**, 2067; (*b*) J. M. Baumes, J. J. Gassensmith, J. Giblin, J. J. Lee, A. G. White, W. J. Culligan, W. M. Leevy, M. Kuno and B. D. Smith, *Nat. Chem.*, 2010, **2**, 1025; (*c*) Q. Wang, X. Jiao, C. Liu, S. He, L. Zhao and X. Zeng, *J. Mater. Chem. B*, 2018, **6**, 4096; (*d*) C. Liu, X. Jia, S. He, L. Zhao and X. Zeng, *Org. Biomol. Chem.*, 2017, **15**, 3947; (*e*) X. Jiao, C. Liu, Q. Wang, K. Huang, S. He, L. Zhao and X. Zeng, *Anal. Chim. Acta*, 2017, **969**, 49; (*f*) X. Wang, L. Cui, N. Zhou, W. Zhu, R. Wang, X. Qian and Y. Xu, *Chem. Sci.*, 2013, **4**, 2936.

3 (*a*) Z. Q. Guo, S. Park, J. Yoon and I. Shin, *Chem. Soc. Rev.*, 2014, **43**, 16; (*b*) R. Weissleder and V. Ntziachristos, *Nat. Med.*, 2003, **9**, 123; (*c*) A. N. Butkevich, G. Lukinavičius, E. D'Este and S. W. Hell, *J. Am. Chem. Soc.*, 2017, **139**, 12378; (*d*) L. Yuan, W. Y. Lin, K. B. Zheng, L. W. He and W. M. Huang, *Chem. Soc. Rev.*, 2013, **42**, 622.

Open Access Article. Published on 14 October 2020. Downloaded on 1/21/2026 2:04:22 AM.
This article is licensed under a Creative Commons Attribution-NonCommercial 3.0 Unported Licence.

4 (*a*) E. David, J. Lejeune, R. S. Pellet, J. Schulz, M. Lemaire and J. Chauvin, *Tetrahedron Lett.*, 2008, **49**, 1860; (*b*) C. Liu, X. Jiao, Q. Wang, K. Huang, S. He, L. Zhao and X. Zeng, *Chem. Commun.*, 2017, **53**, 10727; (*c*) Y. Koide, Y. Urano, K. Hanaoka, T. Terai and T. Nagano, *J. Am. Chem. Soc.*, 2011, **133**, 5680; (*d*) Q. Wang, K. Huang, S. Cai, C. Liu, X. Jiao, S. He, L. Zhao and X. Zeng, *Org. Biomol. Chem.*, 2108, **16**, 7609; (*e*) Q. Wang, X. Jiao, C. Liu, K. Huang, S. He, L. Zhao and X. Zeng, *Org. Biomol. Chem.*, 2018, **16**, 7163; (*f*) C. Liu, Q. Wang, X. Jiao, H. Yao, S. He, L. Zhao and X. Zeng, *Dyes Pigm.*, 2019, **160**, 989; (*g*) W. Piao, K. Hanaoka, T. Fujisawa, S. Takeuchi, T. Komatsu, T. Ueno, T. Terai, T. Tahara, T. Nagano and Y. Urano, *J. Am. Chem. Soc.*, 2017, **139**, 13713.

5 T. Ren, W. Xu, W. Zhang, X. Zhang, Z. Wang, Z. Xiang, L. Yuan and X. Zhang, *J. Am. Chem. Soc.*, 2018, **140**, 7716.

6 (*a*) Z. Tian, B. Tian and J. Zhang, *Dyes Pigm.*, 2013, **99**, 1132; (*b*) H. Liu, Y. Zhang, S. Xia, M. Fang, W. Mazi, Y. Zeng, T. Johnston, A. Pap and R. L. Luck, *Chem. Commun.*, 2018, **54**, 7625; (*c*) J. Gong, C. Liu, X. Jiao, S. He, L. Zhao and X. Zeng, *Spectrochim. Acta, Part A*, 2020, **243**, 118821; (*d*) J. Gong, C. Liu, X. Jiao, S. He, L. Zhao and X. Zeng, *RSC Adv.*, 2020, **10**, 29536.

7 Y. K. Kim, H. H. Ha, J. S. Lee, X. Bi, Y. H. Ahn, S. Hajar, J. J. Lee and Y. T. Chang, *J. Am. Chem. Soc.*, 2010, **132**, 576.

8 (*a*) E. A. Belyaeva, D. Dymkowska, M. R. Wieckowski and L. Wojtczak, *Toxicol. Appl. Pharmacol.*, 2008, **231**, 34; (*b*) E. A. Belyaeva, T. V. Sokolova, L. V. Emelyanova and I. O. Zakharova, *Sci. World J.*, 2012, **2012**, 1.

9 W. R. Vollmer and E. Birckner, *J. Fluoresc.*, 1994, **4**, 65.

10 (*a*) G. E. Cartwright and M. M. Wintrobe, *Am. J. Clin. Nutr.*, 1964, **14**, 224; (*b*) A. V. Davis and T. V. O'Halloran, *Nat. Chem. Biol.*, 2008, **4**, 148; (*c*) S. Lutsenko, *Curr. Opin. Chem. Biol.*, 2010, **14**, 211.

11 (*a*) P. A. Cobine, F. Pierrel and D. R. Winge, *Biochim. Biophys. Acta*, 2006, **1763**, 759; (*b*) L. A. Abriata, L. Banci, I. Bertini, S. Ciofi-Baffoni, P. Gkazonis, G. A. Spyroulias, A. J. Vila and S. Wang, *Nat. Chem. Biol.*, 2008, **4**, 599.

12 R. Uauy, M. Olivares and M. Gonzalez, *Am. J. Clin. Nutr.*, 1998, **67**, 952S.

13 (*a*) D. Y. Sasaki, D. R. Shnek, D. W. Pack and F. H. Arnold, *Angew. Chem.*, 1995, **107**, 994; (*b*) R. Krämer, *Angew. Chem.*, 1998, **110**, 804; (*c*) S. G. Kaler, *Nat. Rev. Neurol.*, 2011, **7**, 15; (*d*) K. M. Davies, J. F. B. Mercer, N. Chen and K. L. Double, *Clin. Sci.*, 2016, **130**, 565.

14 J. Gong, C. Liu, X. Jiao, S. He, L. C. Zhao and X. S. Zeng, *J. Mater. Chem. B*, 2020, **8**, 2343.

15 V. Dujols, F. Ford and A. W. Czarnik, *J. Am. Chem. Soc.*, 1997, **119**, 7386.

16 M. Beija, C. A. M. Afonso and J. M. G. Martinho, *Chem. Soc. Rev.*, 2009, **38**, 2410.

17 *Guidelines for drinking-water quality*, World Health Organization Press, Geneva, 4th edn, 2011, p. 340.

18 US EPA, *National Primary Drinking Water Regulations: EPA 812-Z-94-001*, May 2009.

19 (*a*) Y. Li, Y. Zhao, W. Chan, Y. Wang, Q. You, C. Liu, J. Zheng, J. Li, S. Yang and R. Yang, *Anal. Chem.*, 2015, **87**, 584; (*b*) M. Ren, B. Deng, J. Y. Wang, Z. R. Liu and W. Lin, *J. Mater. Chem. B*, 2015, **3**, 6746; (*c*) A. Atkinson and D. R. Winge, Metal acquisition and availability in the mitochondria, *Chem. Rev.*, 2009, **109**, 4708; (*d*) H. li, R. Zhang, C. Li, B. Huang, T. Yu, X. Huang, X. Zhang, F. Li, H. Zhou and Y. Tian, *Org. Biomol. Chem.*, 2017, **15**, 598.

 This journal is © The Royal Society of Chemistry 2020